Journal of
Mechanics of
Materials and Structures

FRACTAL ELEMENTS

Samer Adeeb and Marcelo Epstein

Volume 4, Nº 5 May 2009

mathematical sciences publishers

JOURNAL OF MECHANICS OF MATERIALS AND STRUCTURES
Vol. 4, No. 5, 2009

FRACTAL ELEMENTS

SAMER ADEEB AND MARCELO EPSTEIN

Self-similar fractals are geometrically stable in the sense that, when generated by a recursive copying process that starts from a basic building block, their final image depends only on the recursive generation process rather than on the shape of the original building block. In this article we show that an analogous stability property can also be applied to fractals as elastic structural elements and used in practice to obtain the stiffnesses of these fractals by means of a rapidly converging numerical procedure. The relative stiffness coefficients in the limit depend on the generation process rather than on their counterparts in the starting unit. The stiffness matrices of the Koch curve, the Sierpiński triangle, and a two-dimensional generalization of the Cantor set are derived and shown to abide by the aforementioned principle.

1. Introduction

It has been pointed out that many natural structures have a fractal-like composition. These structures are subject to different kinds of loading. Trabecular bones, for instance, which are shown to possess a fractal-like structure [Parkinson and Fazzalari 2000], are responsible for load bearing in vertebrates. Collagen fibers, a major constituent of ligaments and cartilage, are responsible for carrying tensile forces in those structures. The fibers themselves have the self similar fractal like composition; they are, in fact, bundles of fibrils, which in turn are bundles of subfibrils. The subfibrils, under an electron microscope, are seen to be bundles of microfibrils which are bundles of tropocollagen [Frank and Shrive 1999]. The venous and arterial systems within an organism can also be seen as self similar fractals [Peitgen et al. 2004]. While most of the studies focusing on fractals discuss the shape and image properties of fractals [Dyson 1978; Avnir et al. 1998], those studies fail to analyze their structural properties: how fractals would behave under loading and how their behavior is affected by their fractal properties. There are some attempts to analytically determine the deformation of fractals under load [Capitanelli and Lancia 2002; Carpinteri et al. 2001; 2004; Carpinteri and Cornetti 2002; Epstein and Śniatyscki 2006] however, those attempts are based on advanced mathematical techniques beyond the scope of structural analysis.

The generation of a fractal image is geometrically stable as the final image of a fractal is independent of the shape of the initial unit of generation. In the case of the Sierpiński gasket (often called the Sierpiński triangle), for example, the shape of the fractal is recognized after a few iterations of the generation process even if the initial generator is not a triangle. In this paper we report that an analogous behavior is observed in the structural form of the stiffness matrix of an elastic fractal-like structure. The final form of the stiffness matrix is, in a certain sense, independent of the stiffness properties of the unit of generation. We also show that this final form can be obtained by applying the principle of structural self-similarity defined previously in [Epstein and Adeeb 2008].

Keywords: fractals, finite element analysis, stiffness matrix, Koch curve, Sierpiński triangle, Cantor set.

2. Generic stiffness matrices

A *structural element* is a load-carrying solid that can be connected to other elements at a finite number of sites only. At these potential connection points (called *nodes* or *joints*) one or more degrees of freedom (DOFs) — generally translations and/or rotations — are singled out. It is in correspondence with these DOFs that forces and/or couples may be applied to the structural element either directly or via the reactions arising from other elements or structural supports. The ordered set of the DOFs of a structural element can be conceived as a vector $\boldsymbol{U}$, called the vector of (element) DOFs. In the theory of linear infinitesimal elasticity, to which we confine our analysis, the *elastic energy* W stored within an element is given by the quadratic form

$$W = \tfrac{1}{2}\boldsymbol{U}^{\mathrm{tr}}\boldsymbol{K}\boldsymbol{U},$$

where $\boldsymbol{K}$ is a symmetric positive-definite matrix. The physical meaning of the entry k_{ij} of the *stiffness matrix* $\boldsymbol{K}$ is as follows. Assuming that all the DOFs have been constrained by means of appropriate supports (one support per DOF), this entry represents the reaction in correspondence with the support number i due to a unit displacement of the support number j. The terms stiffness matrix and stiffness coefficient allude precisely to this physical interpretation.

A necessary condition for a solid to qualify as a structural element is that the stiffness coefficients be bounded in absolute value. Although beyond this limitation and the symmetry of the stiffness matrix (which is a direct consequence of the conservation of energy) it appears that the stiffness coefficients could be arbitrary, it is not difficult to see that this is not the case. Indeed, the elements of each column of the stiffness matrix, corresponding as they do to the complete set of reactions of a structure under no external loads, must constitute a system of forces in equilibrium. Beyond the algebraic conditions resulting from this fact, a structural element may enjoy geometric and material symmetry properties, which may result in further restrictions. The purpose of the remainder of this section is to derive the general reduced forms of the stiffness matrices of a few structural elements taking all these conditions into consideration.

2.1. ***The stiffness matrix of an equilateral triangle.*** Our first example consists of an equilateral triangle confined to deform in its plane. The nodes are identified with the vertices of the triangle and the DOFs consist of the components of the nodal displacements of these nodes. These components may be expressed either in terms of a global coordinate system, as shown in Figure 1, right, or in terms of conveniently chosen local directions, as illustrated in the left half of the same figure. The internal constitution of the element is not specified at this point, but it will be assumed that the material properties enjoy at least the same symmetries as the geometry.

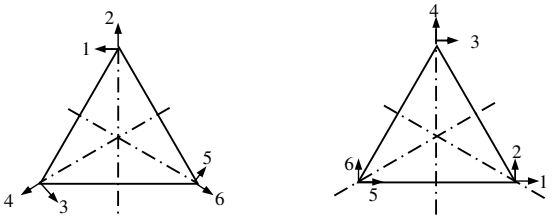

Figure 1. The equilateral triangular element, with local coordinates (left) and global ones (right).

To distinguish between the two options for the DOFs shown in Figure 1, we will denote the corresponding 6×6 stiffness matrices by $\hat{\boldsymbol{K}}^T$ and $\boldsymbol{K}^T$, respectively. (The superscript indicates a triangle and should not be confused with the matrix transposition symbol tr.) By the symmetry of the stiffness matrix, each of these matrices has at most 21 independent coefficients. To implement the extra conditions due to geometric and material symmetry, it is convenient to use the DOFs shown in Figure 1, left. Indeed, it is not difficult to see that in terms of these DOFs the following conditions must hold (assuming that the three axes of geometric symmetry are axes of material symmetry as well):

$$\begin{aligned}
&\hat{k}^T_{11} = \hat{k}^T_{33} = \hat{k}^T_{55} = A^T, && \hat{k}^T_{22} = \hat{k}^T_{44} = \hat{k}^T_{66} = B^T, && \hat{k}^T_{12} = \hat{k}^T_{34} = \hat{k}^T_{56} = 0,\\
&\hat{k}^T_{13} = \hat{k}^T_{35} = \hat{k}^T_{51} = C^T, && \hat{k}^T_{14} = \hat{k}^T_{36} = \hat{k}^T_{52} = D^T, && \hat{k}^T_{23} = \hat{k}^T_{45} = \hat{k}^T_{61} = E^T,\\
& && \hat{k}^T_{24} = \hat{k}^T_{46} = \hat{k}^T_{62} = F^T. &&
\end{aligned} \tag{2-1}$$

Thus, due to geometrical and material symmetries, the total number of independent entries has been reduced to just 6, indicated by the constants appearing on the right-hand sides of (2-1). Moreover, the equilibrium conditions between the entries of each column (j, say) of the stiffness matrix dictate that the following conditions must hold:

$$\begin{aligned}
\hat{k}^T_{1j} - \tfrac{1}{2}(\hat{k}^T_{3j} + \hat{k}^T_{5j}) + \sqrt{3}\tfrac{1}{2}(\hat{k}^T_{4j} - \hat{k}^T_{6j}) = 0,\\
\hat{k}^T_{2j} - \tfrac{1}{2}(\hat{k}^T_{4j} + \hat{k}^T_{6j}) - \sqrt{3}\tfrac{1}{2}(\hat{k}^T_{3j} - \hat{k}^T_{5j}) = 0,\\
\hat{k}^T_{1j} + \hat{k}^T_{3j} + \hat{k}^T_{5j} = 0.
\end{aligned} \tag{2-2}$$

Using (2-2), four of the six coefficients appearing in (2-1) can be written in terms of the other two, say A^t and B^t. The final reduced stiffness matrix with respect to the global DOFs (Figure 1, right) has the form

$$\boldsymbol{K}^T = \begin{pmatrix}
\frac{A^T+3B^T}{4} & \frac{\sqrt{3}(A^T-B^T)}{4} & -\frac{A^T}{2} & \frac{\sqrt{3}(B^T-2A^T)}{2} & \frac{A^T-3B^T}{4} & \frac{\sqrt{3}(3A^T-B^T)}{4}\\
 & \frac{3A^T+B^T}{4} & \frac{\sqrt{3}A^T}{2} & -\frac{B^T}{2} & \frac{\sqrt{3}(B^T-3A^T)}{4} & \frac{B^T-3A^T}{4}\\
 & & A^T & 0 & -\frac{A^T}{2} & -\frac{\sqrt{3}A^T}{2}\\
 & & & B & \frac{\sqrt{3}(2A^T-B^T)}{2} & -\frac{B^T}{2}\\
 & \text{Symmetric} & & & \frac{A^T+3B^T}{4} & \frac{\sqrt{3}(B^T-A^T)}{4}\\
 & & & & & \frac{3A^T+B^T}{4}
\end{pmatrix}. \tag{2-3}$$

2.2. ***The stiffness matrix of a beam.*** The diagram on the right shows a beam element with one axis of (geometric and material) symmetry. To take into consideration bending effects, each node is assigned an extra rotational DOF. Thus, the stiffness matrix of the beam element has a hybrid mixture of coefficients of forces and moments per unit displacements and per unit rotations. Consequently, the length L of the beam

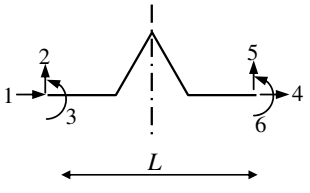

plays a role in the relations between the stiffness coefficients. For convenience, we express the stiffness coefficients k_{ij}^B in terms of homogeneous independent constants. A practical choice of units for these constants is that of the product $E \times I$ (Young's modulus $\times$ moment of inertia $\equiv$ force $\cdot$ length^4/length^2).

By the assumption of one axis of symmetry, the following nine conditions must be satisfied:

$$\begin{aligned} &k_{11}^B = k_{44}^B = A^B, && k_{16}^B = k_{34}^B = -B^B L, && k_{22}^B = k_{55}^B = C^B, \\ &k_{33}^B = k_{66}^B = D^B L^2, && k_{13}^B = k_{46}^B, && k_{12}^B = -k_{54}^B, \\ &k_{15}^B = -k_{24}^B, && k_{23}^B = -k_{56}^B, && k_{26}^B = -k_{35}^B. \end{aligned} \tag{2-4}$$

Moreover, equilibrium of every column of coefficients (equilibrium equations) dictates that, for each j,

$$k_{1j}^B + k_{4j}^B = 0, \qquad k_{2j}^B + k_{5j}^B = 0, \qquad k_{3j}^B + k_{5j}^B L + k_{6j}^B = 0. \tag{2-5}$$

Implementing all these conditions, the general stiffness matrix of a beam with one axis of symmetry becomes

$$\boldsymbol{K}^B = \frac{1}{L^3} \begin{bmatrix} A^B & 0 & B^B L & -A^B & 0 & -B^B L \\ & C^B & \dfrac{C^B L}{2} & 0 & -C^B & \dfrac{C^B L}{2} \\ & & D^B L^2 & -B^B L & -\dfrac{C^B L}{2} & \left(\dfrac{C^B}{2} - D^B\right) L^2 \\ & & & A^B & 0 & B^B L \\ & \text{Symmetric} & & & C^B & -\dfrac{C^B L}{2} \\ & & & & & D^B L^2 \end{bmatrix}. \tag{2-6}$$

2.3. ***The stiffness matrix of a square element.*** Figure 2, left, shows a square element for which every geometric symmetry is also a material symmetry. Each node is assigned two DOFs of displacement in the plane of the square and one rotational DOF in the same plane. Just as in the case of the triangle, it is convenient to implement these symmetries in an adapted coordinate system. The 144 entries of the stiffness matrix $\boldsymbol{K}^s$ are reduced to 78 by symmetry. Following the same procedure as for the previous examples, the geometric and material symmetry translate into a further reduction to 14 independent stiffness coefficients. The equations due to the four axes of symmetry of the square can be expressed as

$$\begin{aligned} &K^S{}_{11} = K^S{}_{44} = K^S{}_{77} = K^S{}_{10\,10} = A^S, \qquad K^S{}_{22} = K^S{}_{55} = K^S{}_{88} = K^S{}_{11\,11} = B^S, \\ &K^S{}_{33} = K^S{}_{66} = K^S{}_{99} = K^S{}_{12\,12} = C^S \times L^2, \end{aligned}$$

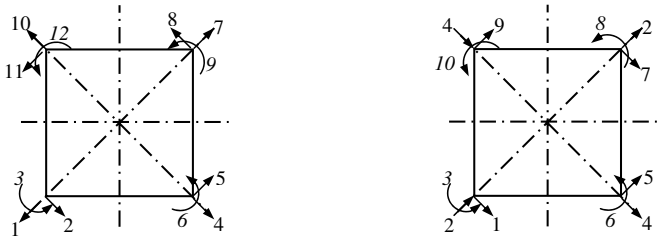

Figure 2. A square element.

$$
\begin{aligned}
&K^S{}_{12} = K^S{}_{13} = K^S{}_{45} = K^S{}_{46} = K^S{}_{78} = K^S{}_{79} = K^S{}_{10\,11} = K^S{}_{10\,12} = K^S{}_{18} = K^S{}_{19}\\
&\qquad = K^S{}_{4\,11} = K^S{}_{4\,12} = K^S{}_{27} = K^S{}_{37} = K^S{}_{6\,10} = K^S{}_{5\,10} = 0,\\
&K^S{}_{14} = K^S{}_{1\,10} = K^S{}_{47} = K^S{}_{7\,10} = D^S, \qquad K^S{}_{25} = K^S{}_{58} = K^S{}_{8\,11} = K^S{}_{2\,11} = E^S,\\
&K^S{}_{28} = K^S{}_{5\,11} = F^S,\\
&K^S{}_{15} = -K^S{}_{1\,11} = K^S{}_{48} = -K^S{}_{24} = K^S{}_{7\,11} = -K^S{}_{57} = K^S{}_{2\,10} = -K^S{}_{8\,10} = G^S,\\
&K^S{}_{16} = -K^S{}_{1\,12} = K^S{}_{49} = -K^S{}_{34} = -K^S{}_{76} = K^S{}_{7\,12} = -K^S{}_{9\,10} = K^S{}_{3\,10} = H^S \times L,\\
&K^S{}_{23} = K^S{}_{56} = K^S{}_{89} = K^S{}_{11\,12} = I^S \times L, \qquad K^S{}_{17} = K^S{}_{4\,10} = J^S,\\
&K^S{}_{2\,12} = K^S{}_{35} = K^S{}_{68} = K^S{}_{9\,11} = K^S{}_{26} = K^S{}_{59} = K^S{}_{8\,12} = K^S{}_{3\,11} = K^S \times L,\\
&K^S{}_{29} = K^S{}_{5\,12} = K^S{}_{38} = K^S{}_{6\,11} = L^S \times L,\\
&K^S{}_{36} = K^S{}_{69} = K^S{}_{9\,12} = K^S{}_{3\,12} = N^S \times L^2, \qquad K^S{}_{39} = K^S{}_{6\,12} = O^S \times L^2.
\end{aligned}
$$

Finally, the columnwise equilibrium conditions effect a further and final reduction to just 9 independent coefficients:

$$
\begin{aligned}
&K^S{}_{2j} + K^S{}_{4j} - K^S{}_{8j} - K^S{}_{10j} = 0, \qquad K^S{}_{5j} + K^S{}_{7j} - K^S{}_{1j} - K^S{}_{11j} = 0,\\
&L \times (K^S{}_{5j} + K^S{}_{8j} + K^S{}_{11j} + K^S{}_{2j})/\sqrt{2} + K^S{}_{3j} + K^S{}_{6j} + K^S{}_{9j} + K^S{}_{12j} = 0.
\end{aligned}
\tag{2-7}
$$

Using the equilibrium equations, five coefficients can be written in terms of the remaining nine coefficients as follows:

$$
\begin{aligned}
&G^S = \tfrac{1}{2}(A^S - J^S), \qquad F^S = B^S - A^S + J^S, \qquad L^S = I^S - 2H^S,\\
&I^S = H^S - K^S - \tfrac{1}{4}\sqrt{2}(-A^S + 2B^S + 2E^S + J^S),\\
&N^S = -\tfrac{1}{2}C^S - \tfrac{1}{2}O^S + \tfrac{1}{4}(-A^S + 2B^S + 2E^S + J^S).
\end{aligned}
\tag{2-8}
$$

As in the case of the beam, the use of hybrid DOFs results in a lack of dimensional homogeneity of the coefficients. For convenience, however, the stiffness coefficients are expressed in terms of 9 constants having the same units and the length of the side, L, makes an explicit appearance wherever needed.

The final reduced stiffness matrix has the form

$$
\boldsymbol{K}^S = \frac{1}{L^3}
\begin{bmatrix}
A^s & 0 & 0 & D^s & G^s & H^sL & J^S & 0 & 0 & D^S & -G^S & -H^SL\\
 & B^S & I^SL & -G^S & E^S & K^SL & 0 & F^S & L^SL & G^S & E^S & K^SL\\
 & & C^SL^2 & -H^SL & K^SL & N^SL^2 & 0 & L^SL & O^SL^2 & H^SL & K^SL & N^SL^2\\
 & & & A^S & 0 & 0 & D^S & G^S & H^SL & J^S & 0 & 0\\
 & & & & B^S & I^SL & -G^S & E^S & K^SL & 0 & F^S & L^SL\\
 & & & & & C^SL^2 & -H^SL & K^SL & N^SL^2 & 0 & L^SL & O^SL^2\\
 & & & & & & A^S & 0 & 0 & D^S & G^S & H^SL\\
 & & & & & & & B^S & I^SL & -G^S & E^S & K^SL\\
 & & \text{Symmetric} & & & & & & C^SL^2 & -H^SL & K^SL & N^SL^2\\
 & & & & & & & & & A^S & 0 & 0\\
 & & & & & & & & & & B^S & I^SL\\
 & & & & & & & & & & & C^SL^2
\end{bmatrix}.
\tag{2-9}
$$

(To avoid complicated expressions within this matrix, (2-8) has not been implemented explicitly.)

2.4. ***Square element with inextensible diagonals.*** For a square with inextensible diagonals, the diagonal displacement of the two vertices across a diagonal are equal and are assigned a single DOF, as seen in Figure 2, right. The stiffness matrix of such a square with respect to the DOFs shown there has 55 coefficients after employing the symmetry of the matrix. The normalization due to the hybrid combination of moments and forces is again utilized. The axes of symmetry can be used to reduce those fifty five coefficients to twelve coefficients as follows:

$$
\begin{aligned}
&K^{IS}{}_{22} = K^{IS}{}_{44} = A^{IS}, \qquad K^{IS}{}_{11} = K^{IS}{}_{55} = K^{IS}{}_{77} = K^{IS}{}_{99} = B^{IS},\\
&K^{IS}{}_{33} = K^{IS}{}_{66} = K^{IS}{}_{88} = K^{IS}{}_{10\,10} = C^{IS} \times L^2,\\
&K^{IS}{}_{12} = K^{IS}{}_{27} = K^{IS}{}_{28} = K^{IS}{}_{23} = K^{IS}{}_{46} = K^{IS}{}_{45} = K^{IS}{}_{4\,10} = K^{IS}{}_{49} = K^{IS}{}_{24} = 0,\\
&K^{IS}{}_{13} = K^{IS}{}_{56} = -K^{IS}{}_{78} = -K^{IS}{}_{9\,10} = D^{IS} \times L,\\
&K^{IS}{}_{15} = -K^{IS}{}_{57} = K^{IS}{}_{79} = -K^{IS}{}_{19} = E^{IS}, \qquad K^{IS}{}_{47} = K^{IS}{}_{14} = K^{IS}{}_{29} = K^{IS}{}_{25} = F^{IS},\\
&K^{IS}{}_{2\,10} = -K^{IS}{}_{26} = K^{IS}{}_{48} = -K^{IS}{}_{34} = G^{IS} \times L,\\
&K^{IS}{}_{16} = K^{IS}{}_{1\,10} = K^{IS}{}_{58} = K^{IS}{}_{53} = -K^{IS}{}_{76}\\
&\qquad = -K^{IS}{}_{7\,10} = -K^{IS}{}_{89} = -K^{IS}{}_{39} = H^{IS} \times L,\\
&K^{IS}{}_{17} = K^{IS}{}_{59} = I^{IS}, \qquad K^{IS}{}_{18} = K^{IS}{}_{5\,10} = -K^{IS}{}_{37} = -K^{IS}{}_{69} = J^{IS} \times L,\\
&K^{IS}{}_{36} = K^{IS}{}_{68} = K^{IS}{}_{8\,10} = K^{IS}{}_{3\,10} = N^{IS} \times L^2, \qquad K^{IS}{}_{38} = K^{IS}{}_{6\,10} = O^{IS} \times L^2.
\end{aligned}
$$

Equilibrium equations for the square in Figure 2, right, have the form

$$
\begin{aligned}
K^{IS}{}_{2j} + K^{IS}{}_{9j} + K^{IS}{}_{5j} = 0, \qquad K^{IS}{}_{1j} + K^{IS}{}_{7j} + K^{IS}{}_{4j} = 0,\\
L(K^{IS}{}_{1j} + K^{IS}{}_{5j} - K^{IS}{}_{7j} - K^{IS}{}_{9j})/\sqrt{2} + K^{IS}{}_{3j} + K^{IS}{}_{6j} + K^{IS}{}_{8j} + K^{IS}{}_{10j} = 0.
\end{aligned}
\tag{2-10}
$$

Using the equilibrium equations, five coefficients can be written in terms of the remaining seven coefficients as follows:

$$
\begin{aligned}
&F^{IS} = -\tfrac{1}{2}A^{IS}, \qquad I^{IS} = -B^{IS} - F^{IS}, \qquad J^{IS} = D^{IS} - G^{IS},\\
&H^{IS} = -D^{IS} + \tfrac{1}{2}G^{IS} + \tfrac{1}{8}\sqrt{2}(A^{IS} - 4B^{IS} - 4E^{IS}),\\
&N^{IS} = -\tfrac{1}{2}\big(\tfrac{1}{4}A^{IS} - B^{IS} + C^{IS} - E^{IS} + O^{IS}\big).
\end{aligned}
\tag{2-11}
$$

The final stiffness matrix has the form

$$
\boldsymbol{K}^{IS} = \frac{1}{L^3}
\begin{bmatrix}
B^{IS} & 0 & D^{IS}L & F^{IS} & E^{IS} & H^{IS}L & I^{IS} & J^{IS}L & -E^{IS} & H^{IS}L\\
 & A^{IS} & 0 & 0 & F^{IS} & -G^{IS}L & 0 & 0 & F^{IS} & G^{IS}L\\
 & & C^{IS}L^2 & -G^{IS}L & H^{IS}L & N^{IS}L^2 & -J^{IS}L & O^{IS}L^2 & -H^{IS}L & N^{IS}L^2\\
 & & & A^{IS} & 0 & 0 & F^{IS} & G^{IS}L & 0 & 0\\
 & & & & B^{IS} & D^{IS}L & -E^{IS} & H^{IS}L & I^{IS} & J^{IS}L\\
 & & & & & C^{IS}L^2 & -H^{IS}L & N^{IS}L^2 & -J^{IS}L & O^{IS}L^2\\
 & & & & & & B^{IS} & -D^{IS}L & E^{IS} & -H^{IS}L\\
 & & \text{Symmetric} & & & & & C^{IS}L^2 & -H^{IS}L & N^{IS}L^2\\
 & & & & & & & & B^{IS} & -D^{IS}L\\
 & & & & & & & & -D^{IS}L & C^{IS}L^2
\end{bmatrix}.
\tag{2-12}
$$

3. Structural analysis of generated fractals

3.1. ***Structural analysis of a Sierpiński gasket.*** The Sierpiński gasket is a fractal generated from an equilateral triangle. The generation process starts by dividing the area inside the equilateral triangle into four similar copies of the original triangle and removing the middle inverted one as shown in Figure 3a. Each of the remaining three copies is again divided into four copies and the middle inverted one is removed and so on ad infinitum. The process is equivalent to starting with a triangle and making two extra copies and placing them as shown in Figure 3b. The new generated structure is then replicated again and the process is repeated ad infinitum. This process of generation is used to generate a Sierpiński gasket from a triangular structural element. A finite element analysis package (ABAQUS 6.6) is utilized to generate a three-node triangle using a plane stress element with a thickness of 1 unit and side dimensions of 1 unit. The three-node triangle is regarded as a structural element rather than a finite element. The stiffness matrix of the generated structure with respect to the three vertices is obtained in every step during the generation process for the triangle by applying a unit deformation in the vertical direction and obtaining the reactions in the corner nodes. Figure 4 shows the generated Sierpiński gasket at the generation step $n = 8$. Since the generated structure obeys the symmetries described in Section 2.1, the generated stiffness matrix has two independent coefficients, A^{T} and B^{T}, which can be calculated from the obtained reactions, per (2-2).

As pointed out, the (isotropic) material properties of the originator (namely, the triangular building block) do not affect the final ratios between the stiffness coefficients of the fractal obtained as limit. We have referred to this property as stability. To check that this is indeed the case, we examine two cases separately. In both cases the Young's modulus of the originator triangle was assumed to be equal to 1 unit, but the Poisson's ratio was set to 0 for the first case and to 0.4999 for the second. The stiffness matrix of the generated structure converges to one single form for both sets. The ratio $B^{\mathrm{T}}/A^{\mathrm{T}}$ stabilizes and reaches the value 3 after a few steps of the generation process indicating that the details of the stiffness

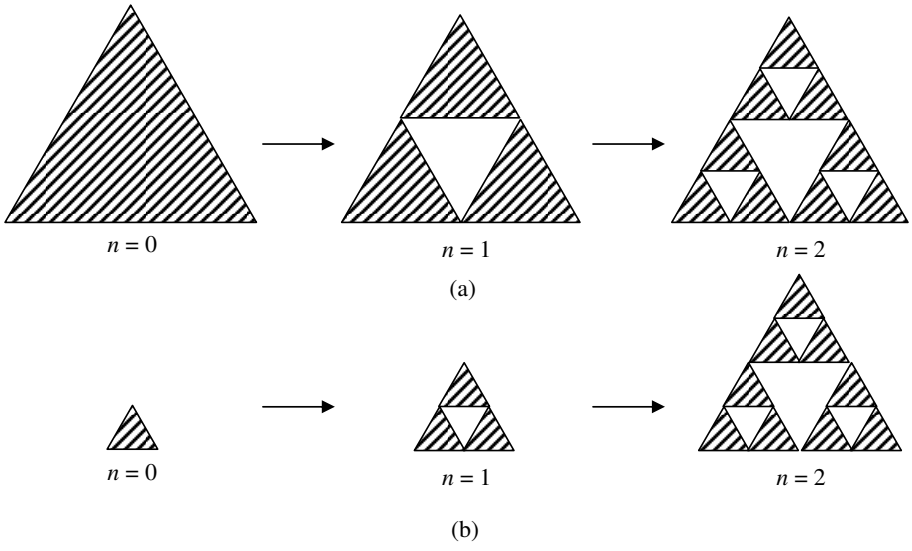

Figure 3. Generation of a Sierpiński gasket by division (a) and by copying (b).

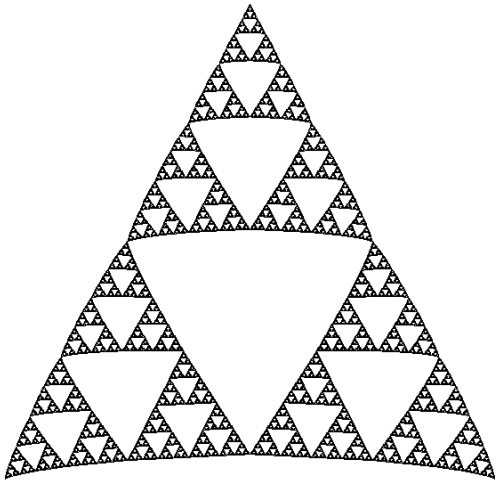

Figure 4. The generated Sierpiński gasket after applying an upward unit deformation at the top vertex while restraining the remaining DOFs. The gasket is shown at the generation step $n = 8$.

of the originator disappear after a few steps of the generation process (see Figure 5a). The generated stiffness matrix for a Sierpiński gasket has only one independent coefficient, namely A^T. The obtained stiffness matrix throughout the generation process appears to be scaled down by the same scaling factor from one step to the next. After a few generation steps, the value of A^T at a generation step n approaches half the value of A^T at the generation step $n - 1$ (see Figure 5b).

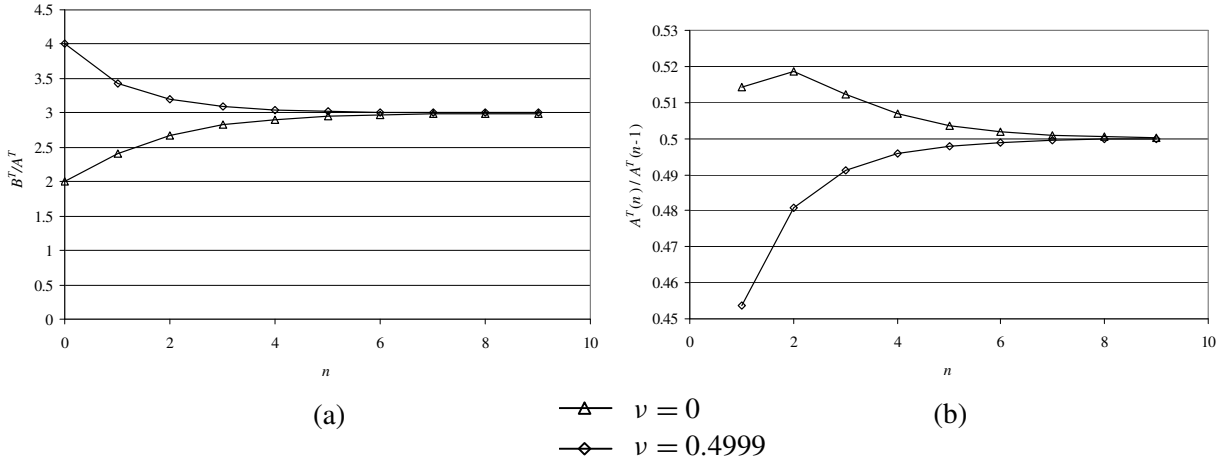

Figure 5. Stability of the stiffness form of a Sierpiński gasket for both sets of stiffness for the originator triangle: (a) the ratio $B^{\mathrm{T}}/A^{\mathrm{T}}$ stabilizes at a value of 3; (b) the ratio $A^{\mathrm{T}}(n)/A^{\mathrm{T}}(n-1)$ stabilizes at a value of 0.5. Each part shows the result for two values of the Poisson's ratio ν.

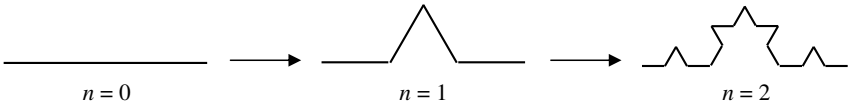

Figure 6. Generation of a Koch curve.

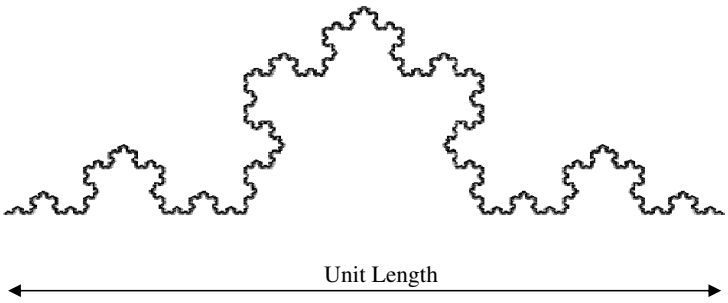

Figure 7. The generated Koch beam at $n = 5$.

3.2. ***Structural analysis of a Koch beam.*** The Koch curve is generated by dividing a line segment into three equal parts, removing the middle part, and replacing it by two copies of itself rotated by an angle of sixty degrees. The process is then repeated for the generated four line segments ad infinitum (see Figure 6). The six-DOF structure thus generated is called the Koch beam. ABAQUS 6.6 was used to generate a Koch beam with unit length as a combination of Euler–Bernoulli elastic beams with a Young's modulus of 1 unit and a moment of inertia of 1 unit. The area of the beams was taken as an arbitrary large number (10000 units) as the deformations are expected to be primarily due to bending. The generated stiffness matrix has four independent coefficients as described in (2-6), namely A^B, B^B, C^B, and D^B. By analyzing (2-6) it is obvious that rows 4 and 6 are sufficient to obtain the four independent coefficients of the stiffness matrix of such a beam. Those independent coefficients can be obtained by applying a unit deformation to DOF number 4 and a unit rotation to DOF number 6 shown (see figure at bottom of page 783). Just as with the Sierpiński gasket, the stiffness form of the generated Koch beam stabilizes after a few generation steps. Each of the ratios of B^B, C^B, and D^B with respect to A^B reaches a limit (see Figure 8a) and the scaling factor (the ratio between the stiffness A^B at a generation step n and the stiffness A^B at the generation step $n-1$) stabilizes at a value of $3/4$ (see Figure 8b). This factor of $3/4$ is only attainable due to keeping the total length of the Koch beam at each generation step n equal to the length at the previous generation step $(n-1)$. It should be noted here that the ratio between A^B at a generation step n and the value of a^B (being the equivalent stiffness of one of the four legs of the Koch beam during the same generation step) is equal to $1/36$. The leg on its own is considered to be in the generation step $n-1$, thus having a higher scaling stiffness, with value $4/3$. The length of the leg is three times less than the length of the whole Koch beam and thus the $1/L^3$ term in the stiffness matrix further increases the stiffness of the leg by a value of 27. The total increase in stiffness of the leg compared to that of the whole Koch beam is equal to 36.

3.3. ***Structural analysis of a two-dimensional modification of the Cantor set.*** An interesting structural fractal, based on a square and reminiscent of the Cantor set, can be obtained as follows. At the generation

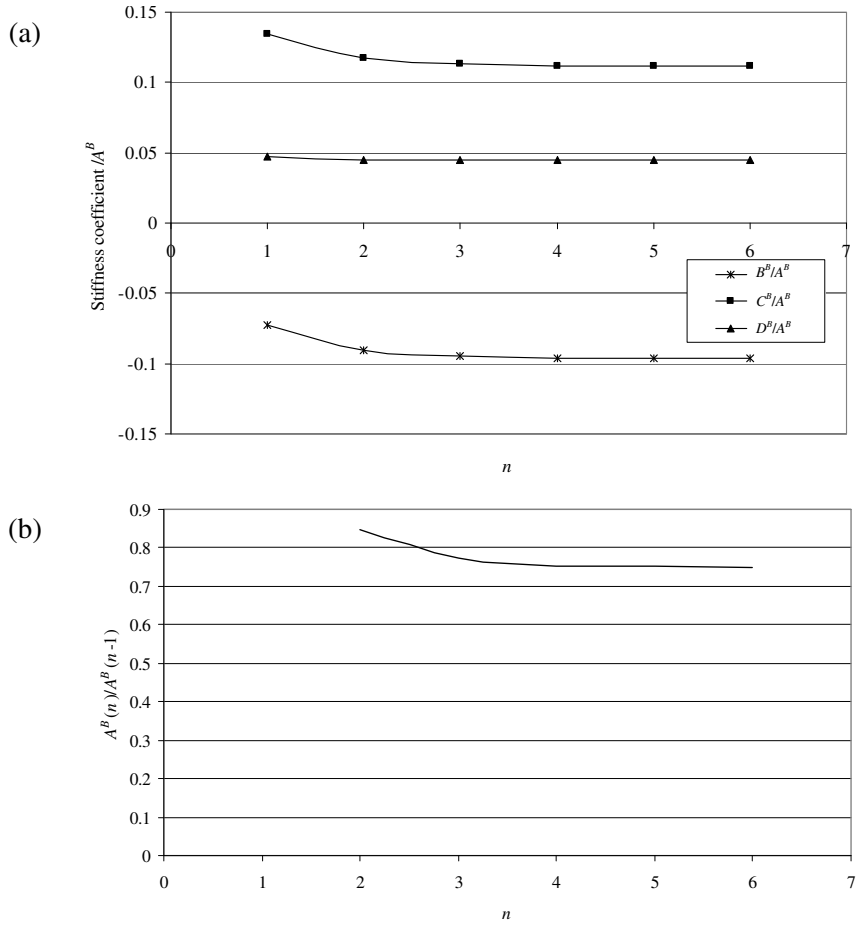

Figure 8. Stability of the stiffness form of a Koch beam. (a) The ratio of each of B^B, C^B, and D^B to A^B stabilizes at a constant value. (b) The ratio $A^B(n)/A^B(n-1)$ stabilizes at a value of 0.75.

step $n = 1$, the square is divided into nine equal squares, four of which are removed (see Figure 9). The removed squares are those involving the middle third of each side of the original square. Taking a closer look at the side, it can be noticed that at the first generation step, the open set $]1/3, 2/3[$ of the line segment [0, 1] representing each side has been removed. In the following generation steps, the process is repeated for every remaining square. As far as the sides of the original square are concerned, this process results in the generation of the Cantor set.

For this structure to be stable, each square should have a rotational DOF at the corner node; hence the need for the stiffness matrix described in Section 2.3. Nine arbitrary values for the stiffness matrix (2-9) were chosen, ensuring that the matrix is positive definite. The chosen stiffness matrix was rotated to appropriate DOFs that can be implemented in a commercial finite element package using the relationship $\boldsymbol{K}^{\text{rotated}} = \boldsymbol{Q}^{\text{tr}} \boldsymbol{K}\, \boldsymbol{Q}$, where $\boldsymbol{Q}$ is the rotation matrix between the two sets of DOFs. ABAQUS 6.6 was used to generate the model of this fractal at different generation steps. Step $n = 0$ represents a square of unit

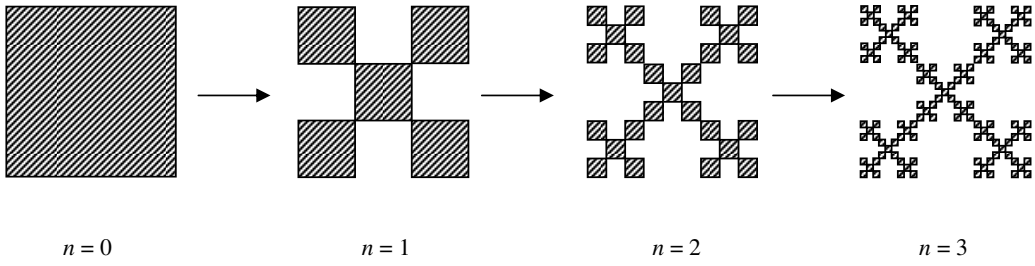

Figure 9. Two-dimensional modification of the Cantor set.

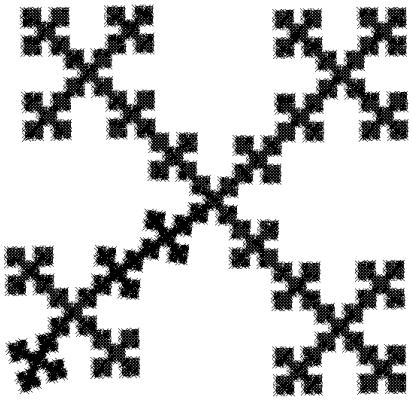

Figure 10. Deformation shape of the two-dimensional Cantor set at $n = 5$ when applying a unit rotation to DOF number 3 and restraining all remaining DOFs at the four corner vertices.

side length with the specified stiffness matrix. Step $n = 1$ represents five squares, each of unit side length and with the specified stiffness matrix. Thus, the total side length of the model grew with the generation steps. The *user element* option was used to input the stiffness matrix for the square unit against the DOFs in a Cartesian coordinate system. By close examination of (2-9), any three columns belonging to the DOFs of one node are sufficient to reproduce the nine coefficients of the matrix. Thus, three separate loading cases were applied on a chosen corner node; two perpendicular unit displacements and a unit rotation. At each generation step and in each loading case, the resulting reactions at the remaining three nodes were obtained and were used to regenerate the stiffness matrix in a Cartesian coordinate system. The stiffness matrix generated was then rotated back to the DOFs shown in Figure 2 and the nine stiffness coefficients of the generated structure were extracted according to (2-9). The ratios of the coefficients with respect to A^S obtained for the different generation steps reveal that seven of the generated coefficients approached zero (see Figure 11). The ratio J^S/A^S on the other hand approached unity. The stiffness entry A^S represents the force needed to extend the diagonal a unit displacement while the stiffness entry J^S represents the reaction to the force A^S on the opposite side of the diagonal. This clearly indicates that the diagonals become infinitely stiff because of the way this fractal is generated; material is always removed during the generation process except from the diagonals. Any force applied in the diagonal direction is totally absorbed by the reaction on the opposite side of the diagonal and all the

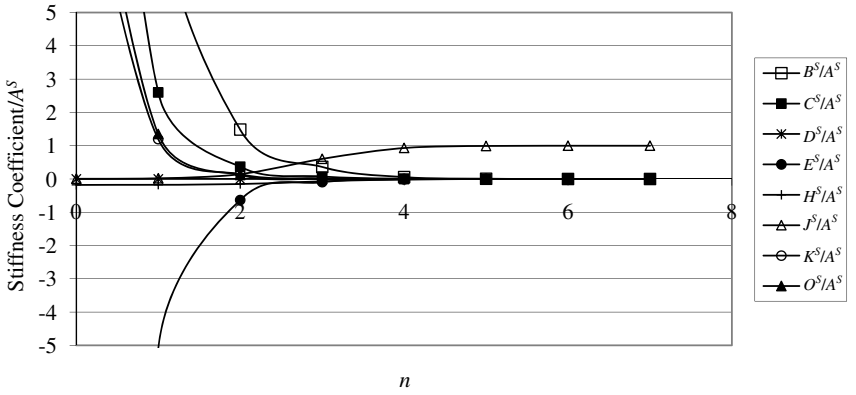

Figure 11. Ratios of stiffness coefficients obtained for the square with respect to the stiffness coefficients A^S.

other reactions to that force are relatively zero. In order to analyze different modes of deformation, the stiffness matrix of a square with inextensible diagonals was introduced in Section 2.4. The new structure with inextensible diagonals will be analyzed in Section 4.3 using the principle of self similarity stated in Section 4.

4. Principle of stiffness self-similarity

It was shown in Section 3 that the stiffness form of fractal structures stabilizes after a few generation steps. It will be shown here that this final form can be achieved by applying the principle of self-similarity to the stiffness matrix of each of the fractals under consideration. A fractal is said to be self-similar if it is an almost disjoint union of shapes that are a reduced copy of the fractal itself. The principle of structural self-similarity was first introduced in [Epstein and Adeeb 2008] and states that for a self-similar fractal the stiffness matrix of $\boldsymbol{K}^f$ is proportional to the stiffness matrix $\boldsymbol{K}^F$ of one of its reduced constituent copies with respect to the corresponding DOFs, namely:

$$\boldsymbol{K}^f = \alpha \boldsymbol{K}^F, \tag{4-1}$$

where α is a constant.

The $n \times n$ stiffness matrix $\boldsymbol{K}^F$ with (where n is the number of DOFs chosen for the fractal) as described in Section 3 contains m independent coefficients after employing all the symmetries and equilibrium conditions. The stiffness matrix $\boldsymbol{K}^f$ of the whole fractal can be constructed by structural analysis assembly procedures of the different units, then condensation to the chosen DOFs of the whole fractal. The assembled stiffness matrix $\boldsymbol{K}^f$ also has $n \times n$ entries. Since the assembled structure has the same symmetries and equilibrium conditions of its units, it will also have m independent entries. These entries will be nonlinear equations of the m independent entries of the stiffness matrix $\boldsymbol{K}^F$. Equation (4-1) can be considered as a system of m equations in $m+1$ unknowns after the introduction of the scaling factor α. Its solution will, therefore, yield the value of α and of the $m-1$ independent ratios between the m independent stiffness values. In order to solve this system of equations, a numerical procedure is employed. Starting with initial values for the m independent coefficients of the stiffness matrix $\boldsymbol{K}^F$,

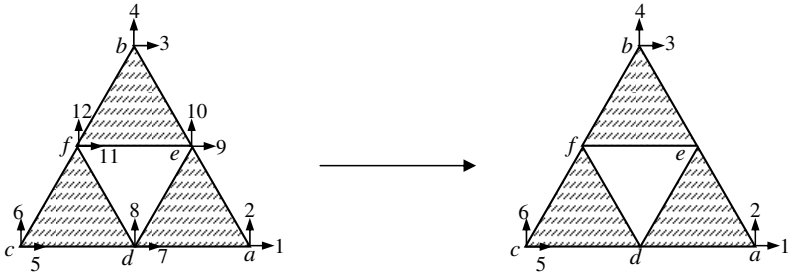

Figure 12. Building up the stiffness of a Sierpiński gasket by assembling three scaled-down copies of the whole structure.

the global stiffness matrix of the whole fractal $\boldsymbol{K}^f$ is assembled. The new m independent coefficients are then extracted from the global stiffness matrix $\boldsymbol{K}^f$ and an average factor α is obtained by dividing the new m independent coefficients of the matrix $\boldsymbol{K}^f$ by the original m independent coefficients of the matrix $\boldsymbol{K}^F$ and averaging the resulting factors. The new independent coefficients divided by the obtained average factor are then used as input for the next step. This process was applied to the fractals under consideration and was shown to lead to the solution obtained in Section 3.

4.1. ***Stiffness self-similarity of the Sierpiński gasket.*** The numerical procedure described above was applied to the Sierpiński gasket. As shown in Figure 12, the equilateral triangle abc is assumed to be composed of three smaller equilateral triangles (aed, ebf, and dfc) with identical 6×6 stiffness matrices $\boldsymbol{K}^{\mathrm{T}}$. Arbitrary positive values are assigned for the coefficients A^{T} and B^{T} in (2-3). The global stiffness matrix has 12×12 entries and can be assembled by combining the three smaller stiffness matrices according to their nodal connectivity. The global stiffness matrix can be reduced to a 6×6 matrix $\boldsymbol{K}^t$ by assuming that there are no external forces applied at nodes d, e or f. Thus, the stiffness matrix $\boldsymbol{K}^t$ of the condensed structure abc can be calculated as follows:

$$\boldsymbol{K}_1\boldsymbol{\Delta}_1 + \boldsymbol{K}_2\boldsymbol{\Delta}_2 = \boldsymbol{F}, \qquad \boldsymbol{K}_2^{\mathrm{tr}}\boldsymbol{\Delta}_1 + \boldsymbol{K}_3\boldsymbol{\Delta}_2 = 0, \qquad \boldsymbol{K}^t = \boldsymbol{K}_1 - \boldsymbol{K}_2\boldsymbol{K}_3^{-1}\boldsymbol{K}_2^{\mathrm{tr}}, \tag{4-2}$$

where tr denotes the transpose, $\boldsymbol{K}_1$ is the first 6×6 entries of the 12×12 global stiffness matrix, Δ_1 is the array of DOFs 1 through 6, $\boldsymbol{K}_2$ is the submatrix containing the entries of rows 1 to 6 and columns 7 to 12 of the global stiffness matrix, Δ_2 is the array of DOFs 7 through 12, $\boldsymbol{F}$ is the array of external forces applied to DOFs 1 through 6, and $\boldsymbol{K}_3$ is the submatrix containing the entries of rows 7 to 12 and columns 7 to 12 of the global stiffness matrix.

After the process of assembly and condensation, the entries ${k^t}_{33}$ and ${k^t}_{44}$ in the matrix $\boldsymbol{K}^t$ are extracted and are divided by the initial arbitrary values of A^{T} and B^{T} to obtain two values that are averaged to obtain a coefficient α. The new values of A^{T} and B^{T} for the next iteration are then taken to be ${k^t}_{33}/\alpha$ and ${k^t}_{44}/\alpha$ respectively. The process was repeated until the values of B^{T} and α stabilized. The results obtained are similar to those obtained in Section 3.1. The ratio of $B^{\mathrm{T}}/A^{\mathrm{T}}$ stabilized at a value of 3 while α converged to a value of 0.5.

4.2. ***Stiffness self-similarity of the Koch beam.*** The assembly of a Koch beam from four similar parts follows the same procedure used for the Sierpiński gasket described in Section 4.1. The beam ab can be assumed to be composed of the assembly of the four beams ac, cd, de, and eb, each having a stiffness

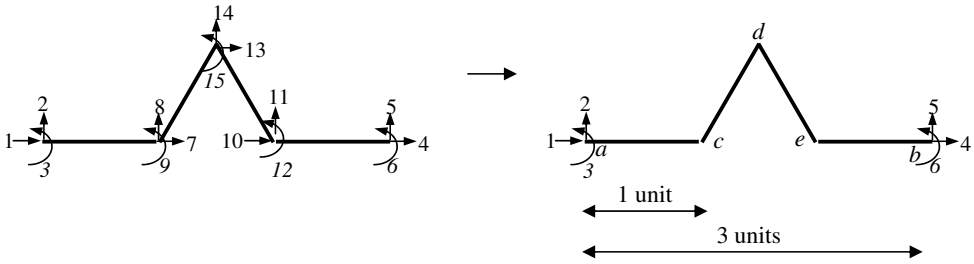

Figure 13. Assembly of a Koch beam from four scaled down copies of the original.

matrix with four independent coefficients according to (2-6). The stiffness matrix K^B for beams cd and de, however, needs to be rotated to the global nodal directions shown in Figure 13. The global assembled stiffness matrix has 15×15 entries and can be reduced to a 6×6 matrix $\boldsymbol{K}^b$ by the equations

$$\boldsymbol{K}_1\boldsymbol{\Delta}_1 + \boldsymbol{K}_2\boldsymbol{\Delta}_2 = \boldsymbol{F}, \qquad \boldsymbol{K}_2^{\mathrm{tr}}\boldsymbol{\Delta}_1 + \boldsymbol{K}_3\boldsymbol{\Delta}_2 = 0, \qquad \boldsymbol{K}^b = \boldsymbol{K}_1 - \boldsymbol{K}_2\boldsymbol{K}_3^{-1}\boldsymbol{K}_2^{\mathrm{tr}}, \tag{4-3}$$

where $\boldsymbol{K}_1$ is the first 6×6 entries of the 15×15 global stiffness matrix, $\boldsymbol{\Delta}_1$ is the array of DOFs 1 through 6, $\boldsymbol{K}_2$ is the submatrix containing the entries of rows 1 to 6 and columns 7 to 15 of the global stiffness matrix, $\boldsymbol{\Delta}_2$ is the array of DOFs 7 through 15, $\boldsymbol{F}$ is the array of external forces applied to DOFs 1 through 6, and $\boldsymbol{K}_3$ is the submatrix containing the entries of rows 7 to 15 and columns 7 to 15 of the global stiffness matrix.

In the first iteration four arbitrary positive values are assumed for the entries A^B, B^B, C^B, and D^B of the stiffness matrix $\boldsymbol{K}^B$. After assembly of the matrix $\boldsymbol{K}^b$ the entries ${k^B}_{11}$ and ${k^B}_{22}$ are extracted and are multiplied by the cube of the length of the whole beam (3 units), then divided by A^B and C^B to obtain two values of the scale factor α. The entry ${k^B}_{13}$ is multiplied by the square of the length of the whole beam and divided by the entry B^B to obtain another value for the scale factor α. A fourth value for α is then obtained by multiplying the entry ${k^B}_{33}$ by the length of the whole beam and then dividing the result by the entry D^B. The four values of α are then averaged and the new values for A^B, B^B, C^B, and D^B are used for the next iteration by using the following entries: ${k^B}_{11}/27\alpha$, ${k^B}_{13}/9\alpha$, ${k^B}_{22}/27\alpha$, and ${k^B}_{33}/3\alpha$ respectively. The results obtained are similar to those obtained in Section 2.2. The values of B^B/A^B, C^B/A^B, D^B/A^B, and α stabilized at -0.09623, 0.1111, 0.0444 and $3/4$ respectively.

4.3. ***Stiffness self-similarity of a two-dimensional modification of the Cantor set.*** The assembly of the two-dimensional Cantor set (Section 3.3) as a union of five scaled copy of itself is shown in Figure 14. The fractal structure $abcd$ with supports on a, b, c, and d can be considered as a union of the fractal structures $aehg$, $fbji$, $himl$, $klod$, and $mncp$ which have stiffnesses that are a scaled copy of the stiffnesses of the global structure. The principle of self-similarity stated can be applied to this fractal as follows: Arbitrary values are given to the nine stiffness entries of the unit square in (2-9). The stiffness matrix is then rotated to the global DOFs shown in Figure 14. After assembly, the global stiffness matrix had 48×48 entries. The stiffness matrix was then reduced into a 12×12 matrix by eliminating the DOFs at nodes e, f, g, h, i, j, k, l, m, n, o, and p as described in Sections 4.1 and 4.2. After reduction, the stiffness matrix was then rotated to the DOFs shown in Figure 14b. The new stiffness and the ratios were then extracted as described in Sections 4.1 and 4.2. Results similar to those described in Section 3.3

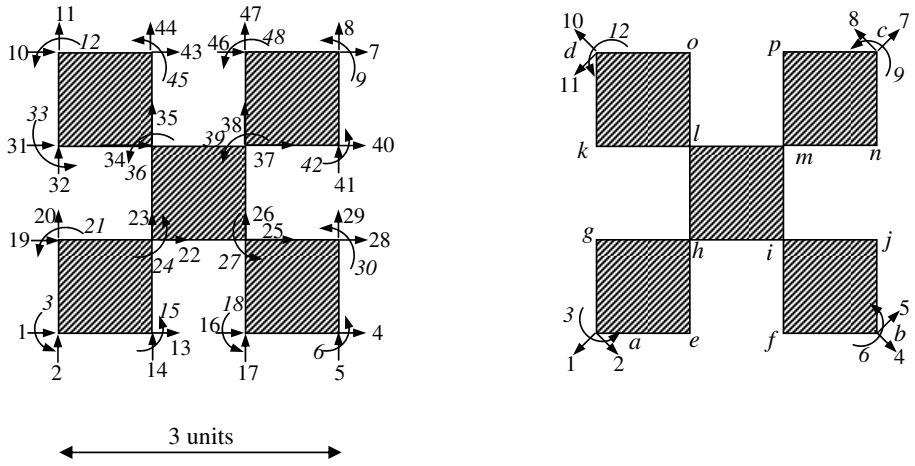

Figure 14. Assembly of the two-dimensional modification of the Cantor set fractal from five scaled down copies of the original.

were obtained using the self-similarity principle. The fractal is infinitely stiff in the diagonal direction with respect to the remaining DOFs. All the stiffness coefficients approached zero except A^S and J^S which had equal values, indicating that the generation of this fractal causes the diagonals to be infinitely stiff compared to other deformation shapes. The ratio between the input stiffness entry $k^s{}_{11}$ of the unit square and the output stiffness entry $K^S{}_{11}$ was found to be 3, which is the ratio of the side length of the output structure to the side length of the input unit square.

The stiffness form of the described fractal in modes of deformation other than along the diagonals can be obtained by applying the principle of self-similarity to the assembled fractal structure in Figure 15. In this case, however, the deformations along the diagonals are considered to be single DOFs and

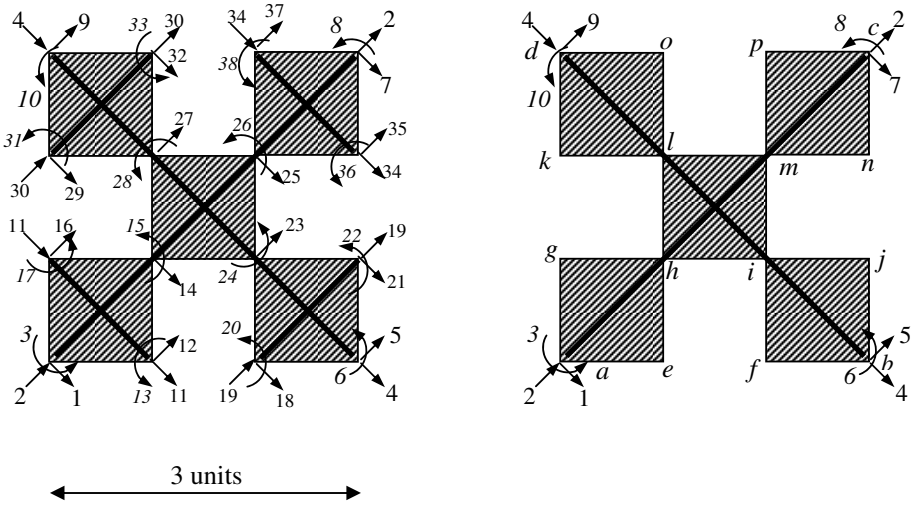

Figure 15. Assembly of the two-dimensional modification of the Cantor set fractal from five scaled down copies of the original, all having inextensible diagonals.

thus the global stiffness matrix has 38×38 entries. The same procedure used for the Koch beam and for the Sierpiński gasket is employed to find the form of the stiffness matrix $\boldsymbol{K}^{IS}$ shown in Equation (2-12) and the ratios between the stiffness coefficients of the global structure and the stiffness coefficients of the unit structure. The final converged ratios of the seven independent coefficients B^{IS}, C^{IS}, D^{IS}, E^{IS}, G^{IS}, and O^{IS} with respect to A^{IS} were equal to 0.40625, 0.078125, -0.15468, -0.09375, -0.17678, and -0.00521. The ratio between the stiffness entry ${k^{IS}}_{22}$ of the initial unit square stiffness matrix $\boldsymbol{K}^{is}$ and the stiffness entry ${K^{IS}}_{22}$ of the global stiffness matrix of the whole structure $\boldsymbol{K}^{IS}$ after assembly and reduction was equal to 27. As the global structure has a length that is 3 times higher than the unit of generation, the length scaling described in Section 3.2 has to be taken into consideration. Thus, the entry ${k^{IS}}_{22}$ is multiplied by the cube of the length of the unit square to obtain a^{IS}, while the entry ${K^{IS}}_{22}$ is multiplied by the cube of the length of the global structure to obtain A^{IS}:

$$\frac{{k^{IS}}_{22}}{{K^{IS}}_{22}} = 27, \qquad \frac{a^{IS}}{L^3_{\text{unit square}}} = {k^{IS}}_{22}, \qquad \frac{A^{IS}}{27L^3_{\text{unit square}}} = {K^{IS}}_{22} = \frac{{k^{IS}}_{22}}{27} = \frac{a^{IS}}{27L^3_{\text{unit square}}}. \tag{4-4}$$

Thus, A^{IS} is equal to a^{IS} and the scaling factor α for this fractal is equal to unity.

5. Conclusions

The geometrical stability of self-similar fractals has been shown previously to be reflected in the fact that the final image of a self-similar fractal is not dependent on the image of the building block but rather on the generation procedure [Peitgen et al. 2004]. In this paper we showed that when we consider the fractals as elastic structures, the stiffness form of such structures will also depend on the generation process rather than on the numerical values of the stiffness coefficients of the building block, as long as it is isotropic. This structural-form stability was shown in three fractal-like structures: the Sierpiński triangle the Koch curve, and a two-dimensional generalization of the Cantor set. For each of those fractals, it was shown that there is a final relationship between the independent entries of the stiffness matrix of the generated fractal. This relationship is shown to be independent of the initial relationship among the entries of the stiffness matrix of the building block and to depend only on the generation process and the geometric and material symmetries of the fractal.

In order to find the relationship between the entries and/or the form of the stiffness matrix of a fractal, the principle of structural self similarity has been previously introduced by Epstein and Adeeb [2008]. The structural self-similarity principle states that the stiffness matrix of a fractal is proportional to the stiffness matrix of a reduced copy of that same fractal, thus a relationship between the entries can be obtained. In this paper we show a numerical algorithm by which this structural self-similarity principle can be applied to obtain those relationships among the stiffness matrix entries. The principle was applied to the Koch curve, the Sierpiński triangle, and a two-dimensional generalization of the Cantor set. The relationship between the stiffness matrix entries obtained for the three fractal structures using the self-similarity principle exactly match the relationship obtained by the structural analysis of the generated fractals.

The question that poses itself is that self-similar fractals in the strict sense as defined by Mandelbrot [1982] are objects that replicate themselves at all scales, but many of the fractal-like objects found in nature have only a finite range in which they are effectively self-similar [Avnir et al. 1998; Parkinson and

Fazzalari 2000]. The results of our analysis show that the structural properties of a fractal as seen in this work (see Figures 5, 8, and 11) reach a very close approximation to their final stabilized values at the iteration step $n = 4$ or 5. It does not really take long for the originator structural properties to disappear and for the fractal behavior to be dominant.

References

[Avnir et al. 1998] D. Avnir, O. Biham, D. Lidar, and O. Malcai, "Is the geometry of nature fractal?", *Science* **279**:5347 (1998), 39–40.

[Capitanelli and Lancia 2002] R. Capitanelli and M. R. Lancia, "Nonlinear energy forms and Lipschitz spaces on the Koch curve", *J. Convex Anal.* **9** (2002), 245–257.

[Carpinteri and Cornetti 2002] A. Carpinteri and P. Cornetti, "A fractional calculus approach to the description of stress and strain localization in fractal media", *Chaos Solitons Fract.* **13**:1 (2002), 85–94.

[Carpinteri et al. 2001] A. Carpinteri, B. Chiaia, and P. Cornetti, "Static-kinematic duality and the principle of virtual work in the mechanics of fractal media", *Comput. Methods Appl. Mech. Eng.* **191**:1–2 (2001), 3–19.

[Carpinteri et al. 2004] A. Carpinteri, B. Chiaia, and P. Cornetti, "The elastic problem for fractal media: basic theory and finite element formulation", *Comput. Struct.* **82**:6 (2004), 499–508.

[Dyson 1978] F. Dyson, "Characterizing irregularity", *Science* **200**:4342 (1978), 677–678.

[Epstein and Adeeb 2008] M. Epstein and S. M. Adeeb, "The stiffness of self-similar fractals", *Int. J. Solids Struct.* **45**:11–12 (2008), 3238–3254.

[Epstein and Śniatyscki 2006] M. Epstein and J. Śniatyscki, "Fractal mechanics", *Physica D* **220** (2006), 54–68.

[Frank and Shrive 1999] C. B. Frank and N. G. Shrive, "Ligaments", pp. 107–126 in *Biomechanics of the musculo-skeletal system*, 2nd ed., edited by B. M. Nigg and W. Herzog, Wiley, Chichester, 1999.

[Mandelbrot 1982] B. Mandelbrot, *The fractal geometry of nature*, W. H. Freeman, San Francisco, 1982.

[Parkinson and Fazzalari 2000] I. H. Parkinson and N. L. Fazzalari, "Methodological principles for fractal analysis of trabecular bone", *J. Microsc.* **198**:2 (2000), 134–142.

[Peitgen et al. 2004] H.-O. Peitgen, H. Jürgens, and D. Saupe, *Chaos and fractals: new frontiers of science*, 2nd ed., Springer, New York, 2004.

Received 28 Dec 2008. Revised 15 May 2009. Accepted 17 May 2009.

SAMER ADEEB: adeeb@ualberta.ca
Department of Civil and Environmental Engineering, University of Alberta, Edmonton, AB T6G 2W2, Canada

MARCELO EPSTEIN: mepstein@ucalgary.ca
Department of Mechanical and Manufacturing Engineering, University of Calgary, 2500 University Drive NW, Calgary, AB T2N 1N4, Canada